A closed-form equation for the local buckling moment of pultruded FRP I-beams in major-axis bending

Francesco ASCIONE,[*a] Luciano FEO,[*b] Marco LAMBERTI,[*c]

Fabio MINGHINI,[**d] Nerio TULLINI[**e]

[*] *Department of Civil Engineering, University of Salerno,*

Via Giovanni Paolo II 132, Fisciano (SA), Italy

[**] *Department of Engineering, University of Ferrara,*

Via Giuseppe Saragat 1, Ferrara, Italy

[a] Corresponding author. E-mail: fascione@unisa.it

[b] E-mail: l.feo@unisa.it

[c] E-mail: malamberti@unisa.it

[d] E-mail: fabio.minghini@unife.it

[e] E-mail: nerio.tullini@unife.it

ABSTRACT

A new closed-form equation for the local instability of pultruded fibre-reinforced plastic beams in bending is derived by substituting suitable buckling approximating functions for compression flange and web into the total potential energy functional. Being obtained from a full-section approach, the equation does not require independent calculations for web and compression flange, which are typical of discrete plate analysis. Moreover, the contribution of the elastic restraint stiffness commonly used to reproduce the web–flange junction behavior naturally arises in the proposed formulation

because of the assumed buckling shape. From comparisons with available experiments on 10 beams and FE solutions for 55 beams, the proposed equation appears to be accurate and reliable.

Keywords: Pultruded beam; Bending; Local buckling; Closed-form equation.

1. INTRODUCTION

Pultruded Fibre-Reinforced Plastic (PFRP) thin-walled profiles can be considered, from a macro-mechanical viewpoint, as linearly elastic, homogeneous, and orthotropic, with the axes of orthotropy coinciding with the principal axes of the cross-sections. Their behavior is highly affected by the relatively low values of the Young's modulus, especially in the transverse direction [1], and of the transverse shear elastic modulus [2, 3], which more or less coincides with that of the polymeric resin and shows a strong time dependency (see [4] and references cited herein). Moreover, warping strains play an important role in the mechanical response of composite thin-walled beams, especially in the case of open sections [5]. These features can provoke non-negligible increases in deformations and deflections with respect to isotropic materials and affect both local and global buckling loads. Finally, post-buckling of pultruded shapes is influenced by the strength of web–flange junctions [1, 6, 7], resin-rich zones from which failure typically propagates [8–10]. As a consequence, PFRP profiles exhibit a complex behavior related to the multi-interaction between shear deformability, non-uniform torsion, and creep, and therefore require suitable modeling criteria.

The flexural-torsional (global) response of PFRP beams has been widely investigated in the literature with regard to both vibrations [11] and buckling [5, 12–15]. The present

paper, instead, focuses on the local bucking phenomenon, starting from a wide overview of the literature, reported in the next section.

2. LITERATURE REVIEW

A brief survey of the literature concerning analytical studies on local buckling of composite structural sections is presented herein. The referenced papers are subdivided into two main categories according to the type of analysis presented.

2.1. Discrete plate analysis

The local buckling analysis of a PFRP shape under axial compression, uniform bending, pure shear, or combinations of the relevant stress states is generally reduced to the analysis of each of the wall segments comprising the shape, which is considered as an individual orthotropic plate that has suitable boundary conditions and is subjected to in-plane loading. In this approach, usually referred to as discrete plate analysis, the longitudinal edges shared by two or more wall segments are usually provided with a continuous elastic restraint, reproducing the stiffening effect due to the adjacent plates.

In [16], the local instability of carbon-fiber-reinforced flanges of I-section beams and columns was analyzed by taking the web restraint coefficient into account.

In [17], a model for the local buckling analysis of I- and box sections was developed, considering the compression flange as an orthotropic plate that was elastically restrained in correspondence with the web–flange junctions. The rotational spring stiffness was assumed to coincide with the bending stiffness of the web in the transverse direction.

The buckling load of orthotropic plates in uniaxial compression, simply supported along the loaded edges and having one of the unloaded edges elastically restrained and

the other free, was found in [18] by solving the governing characteristic transcendental equation numerically. On the basis of a parametric analysis highlighting the role of the coefficient of elastic restraint, R, a procedure is presented to estimate, from test data on FRP beams, the value of R to be used in the local buckling analysis of the compression flange.

Local buckling of box and I-sections under non-uniform bending was analyzed in [19]. In particular, it was assumed that bending is mainly resisted by the flanges, which were subjected to constant compression or tension stresses, whereas non-uniform bending stresses on the web panels were ignored. The web panels were instead subjected to in-plane shear. The local buckling of compression flanges and webs, elastically restrained in correspondence with the web-flange junctions, was then evaluated by solving two transcendental equations simultaneously. Simplified expressions for the buckling strengths were finally obtained using a regression analysis.

Explicit expressions for the local buckling strengths of flange and web panels of box and I-section profiles were reported in [20] and [21], respectively. In particular, an equation for the local buckling of web panels undergoing non-uniform normal stresses and elastically restrained along the unloaded edges was given in [20], seemingly for the first time. Other explicit expressions for web and flange panels of different FRP structural shapes were derived in [22], whereas in [23] the explicit solution to the eigenvalue problem for a composite plate in uniaxial compression with all four edges elastically restrained was reported, followed by an application to honeycomb sandwich structures.

Currently, the best compromise between accuracy and simplicity, and thus practicality in design, is probably represented by the closed-form local buckling

expressions for orthotropic plates derived by Kollár in [24] by combining the buckling loads of plates without bending stiffness, without torsional stiffness and Huber-orthotropic plates. Following the method outlined by Bleich [25] for steel profiles, these expressions, which take account of the rotational restraint offered by adjacent wall segments, were then applied in [26] to the local buckling analysis of thin-walled FRP columns and beams.

Kollár's formulation was adopted by the Italian Design Guide CNR DT 205/2007 [27]. With regard to the local flange buckling of I-section beams, an interesting sensitivity analysis of Kollár's equation was presented in [28, 29], where it was shown that this equation correlates significantly better with the experimental results than those that assume that the half-flanges are simply supported in correspondence with the web–flange junction. Comments on the need to take account of the elastic restraint at the web–flange junction and on the advantages of using Kollár's formulation were reported in [30].

2.2. Analysis of plate assemblies

An approach alternative to that described above consists in applying a variational formulation to the whole thin-walled profile and then minimizing the resulting functional.

Following the work of Bulson [31] on isotropic thin-walled profiles, Zureick and Shih [32] studied the local buckling in FRP beams and columns and deduced the governing stability equations for box and I-section members as special cases. In their proposal, the authors assumed that all plates have the same orthotropic material properties.

In [33], the case of composite I-sections under pure compression was analyzed with regard to both initial buckling and post-buckling, and a numerical solution to the stability equations was finally developed.

In [34], the solution to the general characteristic transcendental buckling equation for FRP profiles subjected to eccentric compression was obtained numerically (pure bending was regarded as a particular case). In particular, the actual stress state on the cross-section was approximated by constant and piecewise constant normal stress distributions applied to flange and web panels, respectively. Different properties were considered for web and flanges.

The formulations presented in [32–34] undoubtedly lead to very accurate reference solutions to the local buckling problem for orthotropic profiles, but they are barely applicable for design purposes. In this context, the development of closed-form expressions would be welcome.

To the authors' knowledge, the only relatively simple closed-form expressions concerning the local buckling of FRP profiles studied as a whole (and not by a discrete plate analysis) are those recently derived in [35] for box, angle-, I-, and C-shaped sections using the Rayleigh energy method [36]. The closed-form local buckling equation for I-sections presented in [36] was proposed again in [37]. These expressions, based on the hypothesis of infinitely long profiles (so as to ignore the influence of the end effects), are restricted to the case of uniform axial compression and assume the same thickness and material properties for all plates comprising the column.

3. MOTIVATION FOR THE STUDY

Kollár's equation [26] is the most widely used expression for the local (flange) buckling resistance of PFRP beams in bending. McCarthy [28] and McCarthy and Bank [29] showed that, in the case of wide-flange I-section beams, the professional bias for Kollár's equation, defined as the ratio of the experimentally determined local buckling strength to the strength predicted by the equation, takes a mean value of 1.20 and exceeds 1.5 for two of the ten profiles investigated (see Table 1, where the reciprocals of this ratio are reported according to a convention more usual in Europe). The test results included in the study were collected from [38], where the profile stiffnesses obtained from coupon tests were also reported. In the case of columns in pure compression, the professional bias of Kollár's equation is 1.07 [29], indicating that the overestimation of the local buckling strength is influenced by the stress distribution on the web.

3.1. Relationship between local buckling moment and bending moment resistance

The Italian Design Guide [27] recommends that the bending moment resistance of PFRP beams in pure bending be determined as

$$M_{\mathrm{Rd}} = \chi_M(\lambda_M) M_{\mathrm{loc,Rd}} \tag{1}$$

where $M_{\mathrm{loc,Rd}}$ is the design value of the local buckling moment and $\chi_M(\lambda_M)$ is a function of non-dimensional slenderness $\lambda_M = \sqrt{M_{\mathrm{loc,Rd}} / M_{\mathrm{FT,Rd}}}$ (with $M_{\mathrm{FT,Rd}}$ being the design value of the flexural-torsional buckling moment), which accounts for the interaction between local and global buckling modes [9].

It can be shown that if $M_{loc,Rd}$ is underestimated by 20 and 50% (in line with the mean and maximum values of the professional bias for Kollár's equation reported by McCarthy [28]), the moment M_{Rd} obtained from Eq. (1) turns out to be underestimated by about 10 and 21%, respectively. Therefore, because of the relation between $M_{loc,Rd}$ and M_{Rd}, it appears evident that an accurate prediction of moment $M_{loc,Rd}$ is required for design purposes.

The main objective of the present study is then the development of a new closed-form equation for I-section beams that provides M_{loc}-predictions that are more accurate than those provided by Kollár's equation. The approach used in the paper is that mentioned in Section 2.2. Therefore, distinct buckling stress calculations for flange and web panels are not required, and the resulting full-section equation can be applied to estimate M_{loc} independently of whether local instability is triggered by compression flange or web.

4. PROPOSED CLOSED-FORM EQUATION

The closed-form expressions developed in this paper apply to I-section beams with overall cross-section depth H, flange breadth b_f, and web and flange thicknesses t_w and t_f, respectively (Fig. 1a). Since the flange and web panels of commercial profiles typically show different mechanical properties [39], subscripts "f" and "w" will be used in the following to refer to flanges and web, respectively. Note that in standard PFRP structural shapes the equality $t_w = t_f$ generally holds, but for generality of the wording it will be assumed that flanges and web have different thicknesses.

The assumptions at the basis of the formulation presented hereinafter are the same as those typically adopted for the local buckling analysis of PFRP sections (see for

example [19, 32, 34]); that is, (1) each of the panels constituting the pultruded shape is a linearly elastic orthotropic plate with the orthotropy axes coinciding with the principal axes of the plate; (2) deformations are small and no geometric imperfection is considered; (3) on buckling, the junctions between adjacent panels remain straight; (4) the original angles between adjacent panels remain unchanged; (5) the wavelengths of the various buckled panels are the same; and (6) instability occurs simultaneously for every panel. Because of assumption no. (4), the buckling shape of the compression flange turns out to be symmetric with respect to the web–flange junction.

For a PFRP beam in major-axis bending, the local buckling moment may be evaluated from the following relation (see [27]):

$$M_{\mathrm{loc}} = W_{\max} f_{\mathrm{loc}} \tag{2}$$

where $W_{\max}$ is the beam section modulus in the bending plane and f_{loc} indicates the critical normal stress. Thin-walled profiles can usually be reduced to their middle surface. Under this assumption, f_{loc} in Eq. (2) corresponds to the stress acting at buckling along the compression flange. At the same time, the tension flange is subjected to constant stress $-f_{\mathrm{loc}}$, whereas the web undergoes a linearly varying stress distribution between $-f_{\mathrm{loc}}$ and f_{loc}.

In the present paper, the critical normal stress will be expressed in the general form:

$$f_{\mathrm{loc}} = k_{\mathrm{loc}} \frac{\pi^2 E_{\mathrm{L,f}}}{12\left(1-\upsilon_{\mathrm{LT,f}}\upsilon_{\mathrm{TL,f}}\right)}\left(\frac{t_{\mathrm{f}}}{b_{\mathrm{f}}}\right)^2 = k_{\mathrm{loc}} \frac{\pi^2 D_{11,\mathrm{f}}}{t_{\mathrm{f}} b_{\mathrm{f}}^2} \tag{3}$$

where $E_{\mathrm{L,f}}$, $\upsilon_{\mathrm{LT,f}}$, and $\upsilon_{\mathrm{TL,f}}$ are the longitudinal elastic modulus and the major and minor in-plane Poisson's ratios of the flanges, respectively, whereas $D_{11,\mathrm{f}}$, whose definition is reported in Table 2, is the longitudinal bending stiffness of the flange panels. Finally,

k_{loc} in Eq. (3) represents a buckling coefficient to be determined by making the total potential energy of the buckled beam stationary.

4.1. Variational formulation

A Cartesian coordinate system (O; x, y) is considered. A generic, rectangular orthotropic plate i is assumed to have one of the vertexes coinciding with the origin O and edges with dimensions a and b parallel to the directions x and y, respectively. If the plate is subjected to an out-of-plane displacement function $w_i(x, y)$, its strain energy, neglecting transverse shear deformations, takes the following form [40]:

$$U_i = \frac{1}{2}\int_0^a \int_0^b \left\{ D_{11,i}\left(\frac{\partial^2 w_i}{\partial x^2}\right)^2 + D_{22,i}\left(\frac{\partial^2 w_i}{\partial y^2}\right)^2 + 2D_{12,i}\left(\frac{\partial^2 w_i}{\partial x^2}\right)\left(\frac{\partial^2 w_i}{\partial y^2}\right) + 4D_{66,i}\left(\frac{\partial^2 w_i}{\partial x \partial y}\right)^2 \right\} dydx \tag{4}$$

where coefficients $D_{11,i}$, $D_{22,i}$, $D_{12,i}$, and $D_{66,i}$ represent the plate bending stiffnesses (see Table 2).

The work done by a constant compressive stress f_x applied to the plate edges parallel to the y-axis can be written as [40]:

$$V_i = f_x t_i \int_0^a \int_0^b \left(\frac{\partial w_i}{\partial x}\right)^2 dydx \tag{5}$$

where t_i indicates the plate thickness. Otherwise, the work done by a normal stress distribution applied to the same edges but varying linearly between compression stress f_x (at $y = 0$) and tension stress $-f_x$ (at $y = b$) is given by [20]:

$$V_i = \frac{1}{2} f_x t_i \int_0^a \int_0^b \left(1 - 2\frac{y}{b}\right)\left(\frac{\partial w_i}{\partial x}\right)^2 dydx \tag{6}$$

For an I-beam in major-axis bending, it is assumed that, at buckling, the tension flange remains undeformed [32]. Therefore the total potential energy, comprising the contributions of the compression flange and web only, can be written as:

$$\Pi = U_{\mathrm{f}} - V_{\mathrm{f}} + U_{\mathrm{w}} - V_{\mathrm{w}} \tag{7}$$

where, for a beam of length L corresponding to one single half-wave in the buckling shape, U_{f} and V_{f} are obtained by doubling Eqs. (4) and (5), respectively, written for $i = \mathrm{f}$, $a = L$, and $b = b_{\mathrm{f}}/2$. Moreover, U_{w} and V_{w} follow from Eqs. (4) and (6), respectively, for $i = \mathrm{w}$, $a = L$, and $b = H - t_{\mathrm{f}} = b_{\mathrm{w}}$.

The local buckling stress for a given L, $f_{\mathrm{loc},L}$, corresponds to the value of f_x that minimizes Eq. (7).

4.2. Assumed buckling shape

Suitable displacement fields w_i must be substituted into Eqs. (4)–(6) to obtain a reliable prediction of the local buckling stress. In this paper, the buckling shape is approximated using sinusoidal and polynomial functions.

To express functions w_i for compression flange and web, three local coordinate systems are introduced, with the origin placed at the web–flange junction (Fig. 1a).

With regard to the buckling displacements in the plane of the beam cross-section, the cubic shape function proposed in [21, 22] is used for each of the half-flanges, whereas the product of a sinusoidal function with a linear polynomial is proposed for the web. The resulting buckling approximating functions can be written as (see Fig. 1b):

$$w_{\mathrm{f}j} = \alpha\left\{(1-\omega)\frac{y_{\mathrm{f}j}}{(b_{\mathrm{f}}/2)} + \omega\left[\frac{3}{2}\left(\frac{y_{\mathrm{f}j}}{(b_{\mathrm{f}}/2)}\right)^2 - \frac{1}{2}\left(\frac{y_{\mathrm{f}j}}{(b_{\mathrm{f}}/2)}\right)^3\right]\right\}\sin\left(\frac{\pi x}{L}\right) \tag{8}$$

$$\text{for } y_{\mathrm{f}j} \in [0, b_{\mathrm{f}}/2],\ j = 1, 2$$

$$w_{\mathrm{w}} = \alpha(1-\omega)\frac{b_{\mathrm{w}}}{\pi(b_{\mathrm{f}}/2)}\left(\frac{y_{\mathrm{w}}}{b_{\mathrm{w}}}-1\right)\sin\left(\frac{\pi y_{\mathrm{w}}}{b_{\mathrm{w}}}\right)\sin\left(\frac{\pi x}{L}\right) \qquad \text{for } y_{\mathrm{w}} \in [0, b_{\mathrm{w}}] \tag{9}$$

where α represents the amplitude of the flange buckling shape, whereas $\omega \in [0,1]$ is a constant coefficient to be determined by imposing suitable boundary conditions. Note that, for $\omega = 0$, Eq. (8) yields zero curvature in the flange transverse direction. Moreover, for $\omega = 1$, no rotation is allowed at the web–flange junction in compression, leading, from Eq. (9), to $w_{\mathrm{w}} = 0$ everywhere.

It can readily be observed that Eqs. (8) and (9) satisfy the boundary conditions $w_{\mathrm{fj}}(x, 0) = w_{\mathrm{w}}(x, 0) = 0$ and $\left[\partial w_{\mathrm{fj}}/\partial y_{\mathrm{fj}}\right]_{y_{\mathrm{fj}}=0} = \left[\partial w_{\mathrm{w}}/\partial y_{\mathrm{w}}\right]_{y_{\mathrm{w}}=0}$ at the web–flange junction in compression. Moreover, Eq. (9) also satisfies the boundary conditions $w_{\mathrm{w}}(x, b_{\mathrm{w}}) = 0$ and $\left[\partial w_{\mathrm{w}}/\partial y_{w}\right]_{y_{w}=b_{\mathrm{w}}} = 0$ at the web–flange junction in tension.

The moment equilibrium at the web–flange junction in compression yields:

$$24\omega D_{22,\mathrm{f}}/b_{\mathrm{f}}^2 = 4(1-\omega)D_{22,\mathrm{w}}/(b_{\mathrm{f}}b_{\mathrm{w}}) \tag{10}$$

from which ω is obtained in the form:

$$\omega = \left[1 + 6c_{22}(b_{\mathrm{w}}/b_{\mathrm{f}})\right]^{-1} \tag{11}$$

where coefficient c_{22} takes the definition reported in Table 2.

4.3. Local buckling stress

Substituting Eqs. (8) and (9) into Eq. (7) and making the total potential energy stationary yield the critical stress $f_{\mathrm{loc},L}$ for a given value of half-wave length L. If $f_{\mathrm{loc},L}$ is expressed in the same form as Eq. (3), the corresponding buckling coefficient, $k_{\mathrm{loc},L}$, takes the following expression:

$$k_{\mathrm{loc},L}=\frac{4b_{\mathrm{f}}^{2}t_{\mathrm{f}}}{c_{12}L^{2}\left(140b_{\mathrm{w}}^{3}t_{\mathrm{w}}F_{\omega 4}+\pi^{4}b_{\mathrm{f}}^{3}t_{\mathrm{f}}F_{\omega 3}\right)}\left\{35L^{4}\left(144b_{\mathrm{w}}\omega^{2}c_{22}+b_{\mathrm{f}}F_{\omega 2}\right)/b_{\mathrm{f}}b_{\mathrm{w}}\right.$$
$$\left.+L^{2}\left[70b_{\mathrm{w}}F_{\omega 5}c_{32,\mathrm{w}}+\pi^{2}b_{\mathrm{f}}\left(168\omega^{2}c_{32}-420\omega c_{122}+840c_{62}\right)\right]+35b_{\mathrm{w}}^{3}F_{\omega 1}c_{12,\mathrm{w}}+\pi^{4}b_{\mathrm{f}}^{3}c_{12}F_{\omega 3}/4\right\} \tag{12}$$

with c_{12}, c_{32}, c_{62}, c_{122}, $c_{12,\mathrm{w}}$, $c_{32,\mathrm{w}}$, and $F_{\omega i}$ (i = 1, ..., 5) being coefficients reported in Table 2. From minimization of $k_{\mathrm{loc},L}$ with respect to L, the half-wave length $L_{\min}$ satisfying the relation $\partial k_{\mathrm{loc},L}/\partial L=0$ is obtained in the form:

$$L_{\min}=\left\{\frac{b_{\mathrm{f}}b_{\mathrm{w}}\left[140b_{\mathrm{w}}^{3}F_{\omega 1}+\pi^{4}b_{\mathrm{f}}^{3}F_{\omega 3}c_{11}\right]}{140\left[b_{\mathrm{f}}F_{\omega 2}+144b_{\mathrm{w}}\omega^{2}c_{22}\right]}c_{12,\mathrm{w}}\right\}^{1/4} \tag{13}$$

Finally, substituting Eq. (13) into Eq. (12) leads to the following expression for the minimum buckling coefficient:

$$k_{\mathrm{loc}}=\frac{4b_{\mathrm{f}}^{2}t_{\mathrm{f}}}{c_{12}\left(140b_{\mathrm{w}}^{3}t_{\mathrm{w}}F_{\omega 4}+\pi^{4}b_{\mathrm{f}}^{3}t_{\mathrm{f}}F_{\omega 3}\right)}\left[70b_{\mathrm{w}}F_{\omega 5}c_{32,\mathrm{w}}+\pi^{2}b_{\mathrm{f}}\left(168\omega^{2}c_{32}-420\omega c_{122}\right.\right.$$
$$\left.\left.+840c_{62}\right)+\sqrt{35c_{12,\mathrm{w}}\left(140b_{\mathrm{w}}^{3}F_{\omega 1}+\pi^{4}b_{\mathrm{f}}^{3}F_{\omega 3}c_{11}\right)\left(144b_{\mathrm{w}}\omega^{2}c_{22}+b_{\mathrm{f}}F_{\omega 2}\right)/b_{\mathrm{f}}b_{\mathrm{w}}}\right] \tag{14}$$

In conclusion, the present proposal for estimating the local buckling moment for PFRP I-section beams relies upon Eq. (2) in conjunction with Eqs. (3) and (14) for local buckling stress f_{loc} and coefficient k_{loc}, respectively, and with coefficient ω computed from Eq. (11).

The assumption that ω = 0 does not allow the moment equilibrium at the web–flange junction in compression to be satisfied locally, and Eq. (14) reduces to:

$$k_{\mathrm{loc0}}=\frac{2b_{\mathrm{f}}^{2}t_{\mathrm{f}}\left\{b_{\mathrm{w}}\left(3+2\pi^{2}\right)c_{32,\mathrm{w}}+12\pi^{2}b_{\mathrm{f}}c_{62}+\sqrt{c_{12,\mathrm{w}}\left(33+2\pi^{2}\right)\left[b_{\mathrm{w}}^{3}\left(2\pi^{2}-3\right)+\pi^{4}b_{\mathrm{f}}^{3}c_{11}\right]/b_{\mathrm{w}}}\right\}}{c_{12}\left[b_{\mathrm{w}}^{3}t_{\mathrm{w}}\left(\pi^{2}-6\right)+\pi^{4}b_{\mathrm{f}}^{3}t_{\mathrm{f}}\right]}. \tag{15}$$

5. VALIDATION OF THE PROPOSED EQUATION

Reported in this section are the comparisons of the proposed equation with available experimental results and closed-form equations as well as with finite element (FE) solutions. The acronym "PA" will be used in the following to indicate the results of the present analysis.

5.1. Comparison with available experimental data

The present formulation is compared in Table 1 with the experimental results reported in [28]. In particular, the mean value of the ratio r_{PA} between the local buckling moment obtained from Eqs. (2), (3), (11), and (14) ($M_{loc,PA}$) and the experimental buckling moment ($M_{loc,exp}$) is approximately 0.98, a value significantly closer to unity than the mean value of the ratio $r_{Ko} = M_{loc,Ko}/M_{loc,exp}$ (= 0.85), with $M_{loc,Ko}$ being the local buckling moment provided by Kollár's equation. The coefficients of variation (COVs) of r_{PA} and r_{Ko} are substantially coincident.

5.2. Numerical validation

The effectiveness of the proposed formulation is also verified by comparison with the FE-computed local buckling stresses. For this purpose, several FE models of simply supported PFRP beams are developed using ABAQUS [41]. In particular, four-node plate elements S4 are adopted. The constitutive model adopted to describe the beam behavior was the transversally isotropic one. An orthotropic constitutive model, with the orthotropy axes parallel to the principal beam axes, is assigned to each element.

At the beam end sections, whilst flexural rotations are left free, in-plane displacements are prevented at each node in order to reproduce the simply supported

configuration. Moreover, to avoid any possible rigid body motion in the beam longitudinal direction, axial displacement of the midspan cross-section centroid is prevented. Finally, in order to avoid flexural-torsional instability, displacements of the web–flange junctions in the transverse direction are fixed.

Taking account of the actual flange thickness, an offset locating the meshes on the inner surfaces of the flanges is introduced, making it possible to avoid overlapping web and flanges at the web–flange junctions.

Uniform major-axis bending is reproduced by means of linearly varying normal stress distributions applied at the end sections as depicted in Fig. 2. The critical stress associated with the first local buckling mode, $f_{\mathrm{loc,FEM}}$, is searched for using an eigenvalue analysis.

A preliminary convergence test on the beam referred to as V8A in Table 1 is performed to define the optimal mesh to be used (see Table 3). The mesh finally adopted is composed of 20 and 18 subdivisions along each of the flanges and the web, respectively, and 274 subdivisions along the span length, resulting in 15892 finite elements (mesh #6 in Table 3). A typical local buckling shape obtained from the FE analysis is shown in Fig. 3.

Using the same FE discretization, all beams of Table 1 are analyzed and the results are reported in Table 4 in terms of local buckling stress $f_{\mathrm{loc,FEM}}$. Critical stresses $f_{\mathrm{loc,exp}}$ and $f_{\mathrm{loc,PA}}$ obtained from the experiments [28] and proposed formulation, respectively, and the ratios $r_{f,\mathrm{exp}} = f_{\mathrm{loc,exp}}/f_{\mathrm{loc,FEM}}$ and $r_{f,\mathrm{PA}} = f_{\mathrm{loc,PA}}/f_{\mathrm{loc,FEM}}$ are reported in the same table. Taking account of all possible sources of uncertainty affecting the experimental results, as well as the estimates of material properties reported in Table 1 (see [28, 38]), which do not consider possible differences between flange and web properties and, for

vinylester beams, were obtained from coupon data from two actual beams and then averaged for all eight beams, a good agreement between the FE analysis and experimental results is obtained.

Therefore, FE models such as that described above can be regarded as the reference for assessing the predictive capacity of the proposed formulation. With regard to the ten beams of Table 1, the ratio $r_{f,\mathrm{PA}}$ takes a mean value and a COV of 1.053 and 0.070, respectively (Table 4), indicating a very good agreement.

For a deeper assessment of the proposed equations, a parametric analysis is finally carried out. A total of 55 beams, comprising wide-flange (WF) and narrow-flange (NF) profiles, are investigated. In particular, with regard to WF beams (Table 5), eight property sets are considered, in conjunction with three different values of the cross-section thickness (t_i, i = 1, ..., 3) and two values of the in-plane shear modulus (G_j, j = 1, 2), resulting in 48 PFRP profiles. These profiles are referred to as WF(X-t_i-G_j), with X being the integer part of the transverse Young's modulus of the flanges, $E_{\mathrm{T,f}}$, expressed in gigapascals. With regard to NF beams (Table 6), seven different profiles are considered. These profiles are referred to as NF(X_1-X_2-X_3), with X_1, X_2, and X_3 indicating the integer parts of cross-section depth and wall thickness in millimeters and the transverse Young's modulus of the web (E_{Tw}) in gigapascals, respectively.

The span lengths of the profiles analyzed are so large that the number of half-waves in the first local buckling shape ranges between 8 and 20. Therefore, the FE-computed buckling stress can be regarded as a very accurate approximation of the minimum local buckling stress.

The results of the comparison between the present analysis and FE models are summarized in Fig. 4 (data points indicated by solid circles) in terms of the ratio

$f_{loc,pred}/f_{loc,FEM}$ between the predicted and FE-computed buckling stresses. Reported in the same figure is an analogous ratio but with $f_{loc,pred}$ referred to Kollár's equation (data points indicated by open circles). In particular, the mean values of $f_{loc,pred}/f_{loc,FEM}$ are 0.966 (thick solid line in Fig. 4) and 0.827 (dashed line in Fig. 4) in the cases of the present analysis and Kollár's equation, respectively. The coefficients of variation for the two cases are 0.042 and 0.044. In conclusion, at equal scatter, the proposed equation is more accurate.

Assuming that $\omega = 0$ and then calculating the buckling coefficient from Eq. (15) rather than from Eq. (14) produces an increase in the buckling stress. In particular, $f_{loc,pred}/f_{loc,FEM}$ takes a mean value of 1.036, whereas the coefficient of variation becomes 0.057.

6 CONCLUSIONS

A new closed-form equation for the local buckling moment of pultruded FRP beams in bending is derived using suitable displacement functions for compression flange and web in the total potential energy expression. Being obtained from a full-section approach, the equation does not require independent calculations for web and compression flange, which are typical of discrete plate analysis.

Comparisons with available experiments on 10 beams and FE solutions for 55 beams indicate that the proposed equation is very accurate and reliable.

A simplified version of the buckling coefficient proposed, based on the assumption of zero curvature in the buckled flange, is proved to be satisfactory from a technical viewpoint. Its implementation into the Italian Design Guide [27] is suggested.

ACKNOWLEDGMENTS

The present investigation was developed in the framework of the Research Program FAR 2014 of the University of Ferrara. Moreover, the analyses were developed within the activities of the (Italian) University Network of Seismic Engineering Laboratories (ReLUIS) in the research program funded by the (Italian) National Civil Protection, "Progetto Esecutivo 2015", Research Line "Innovative Materials".

REFERENCES

[1] Turvey GJ, Zhang Y. A computational and experimental analysis of the buckling, postbuckling and initial failure of pultruded GRP columns. Comput Struct 2006; 84(22/23): 1527–37.

[2] Mottram JT. Shear modulus of standard pultruded fiber reinforced plastic material. J Compos Constr 2004; 8(2): 141–7.

[3] Minghini F, Tullini N, Laudiero F. Identification of the short-term full-section moduli of pultruded FRP profiles using bending tests. J Compos Constr 2014; 18(1), DOI: 10.1061/(ASCE)CC.1943-5614.0000391.

[4] Sá MF, Gomes AM, Correia JR, Silvestre N. Creep behavior of pultruded GFRP elements – Part 1: Literature review and experimental study. Compos Struct 2011; 93(10): 2450–9.

[5] Cortínez VH, Piovan MT. Stability of composite thin-walled beams with shear deformability. Comput Struct 2006; 84(15/16): 978–90.

[6] Feo L, Mosallam AS, Penna R. Mechanical behavior of web–flange junctions of thin-walled pultruded I-profiles: an experimental and numerical evaluation. Compos Part B: Eng 2013; 48: 18–39.

[7] Mosallam AS, Feo L, Elsadek A, Pul S, Penna R. Structural evaluation of axial and rotational flexibility and strength of web–flange junctions of open-web pultruded composites. Compos Part B: Eng 2014; 66: 311–27.

[8] Bank LC, Yin J. Failure of web-flange junction in postbuckled pultruded I-beams. J Compos Constr 1999; 3(4): 177–84.

[9] Laudiero F, Minghini F, Tullini N. Postbuckling failure analysis of pultruded FRP beams under uniform bending. Compos Part B: Eng 2013; 54: 431–8.

[10] Laudiero F, Minghini F, Tullini N. Buckling and postbuckling finite-element analysis of pultruded FRP profiles under pure compression. J Compos Constr 2014; 18(1), DOI: 10.1061/(ASCE)CC.1943-5614.0000384.

[11] Minghini F, Tullini N, Laudiero F. Vibration analysis of pultruded FRP frames with semi-rigid connections. Eng Struct 2010; 32(10): 3344–54.

[12] Davalos JF, Qiao P, Salim HA. Flexural-torsional buckling of pultruded fiber reinforced plastic composite I-beams: experimental and analytical evaluations. Compos Struct 1997; 38(1–4): 241–50.

[13] Vo TP, Lee J. Flexural-torsional behaviour of thin-walled composite box beams using shear-deformable beam theory. Eng Struct 2008; 30(7): 1958–68.

[14] Ascione F. Influence of initial geometric imperfections in the lateral buckling problem of thin walled pultruded GFRP I-profiles. Compos Struct 2014: 112, 85–99.

[15] Mancusi G, Ascione F, Lamberti M. Pre-buckling behavior of composite beams: A mechanical innovative approach. Compos Struct 2014; 117: 396–410.

[16] Webber JPH, Holt PJ, Lee DA. Instability of carbon fibre reinforced flanges of I section beams and columns. Compos Struct 1985; 4(3): 245–65.

[17] Barbero EJ, Raftoyiannis IG. Local buckling of FRP beams and columns. J Mater Civil Eng 1993; 5(3), 339–55.

[18] Bank LC, Yin J. Buckling of orthotropic plates with free and rotationally restrained unloaded edges. Thin Wall Struct 1996; 24(1): 83–96.

[19] Qiao P, Davalos JF, Wang J. Local buckling of composite FRP shapes by discrete plate analysis. J Struct Eng, ASCE 2001; 127(3): 245–55.

[20] Qiao P, Zou G. Local buckling of elastically restrained fiber-reinforced plastic plates and its application to box sections. J Eng Mech, ASCE 2002; 128(12): 1324–30.

[21] Qiao P, Zou G. Local buckling of composite fiber-reinforced plastic wide-flange sections. J Struct Eng, ASCE 2003; 129(1): 125–9.

[22] Qiao P, Shan L. Explicit local buckling analysis and design of fiber-reinforced plastic composite structural shapes. Compos Struct 2005; 70(4): 468–83.

[23] Shan L, Qiao P. Explicit local buckling analysis of rotationally restrained composite plates under uniaxial compression. Eng Struct 2008; 30(1): 126–40.

[24] Kollár LP. Buckling of unidirectionally loaded composite plates with one free and one rotationally restrained unloaded edge. J Struct Eng, ASCE 2002; 128(9): 1202–11.

[25] Bleich F. Buckling strength of metal structures. New York: McGraw-Hill Book Company; 1952.

[26] Kollár LP. Local buckling of fiber reinforced plastic composite structural members with open and closed cross sections. J Struct Eng, ASCE 2003; 129(11): 1503–13.

[27] CNR, National Research Council of Italy. CNR-DT 205/2007: Guide for the design and construction of structures made of thin FRP pultruded elements; 2008. Available online at <http://www.cnr.it>.

[28] McCarthy MJ. Professional factors for an LRFD standard for pultruded beams. MSc thesis, University of Wisconsin–Madison, 2009.

[29] McCarthy MJ, Bank LC. Sensitivity studies on local flange buckling equations for pultruded beams and columns. In: Ye L, Feng P, Yue Q, editors. Advances in FRP composites in civil engineering, Proc 5th Int Conf FRP Composites in Civil Engineering (CICE 2010). Beijing: Springer; 2010, 115–8.

[30] Mottram JT. Determination of critical load for flange buckling in concentrically loaded pultruded columns. Compos Part B: Eng 2004; 35(1): 35–47.

[31] Bulson PS. The stability of flat plates. London: Chatto & Windus; 1970.

[32] Zureick A, Shih B. Local buckling of fiber-reinforced polymeric structural members under linearly-varying edge loading—Part 1. Theoretical formulation. Compos Struct 1998; 41(1): 79–86.

[33] Papila M, Akgün MA. Post-buckling of composite I-sections. Part 1: Theory. J Compos Mater 2001; 35(9): 774–96.

[34] Ragheb WF. Local buckling analysis of pultruded FRP structural shapes subjected to eccentric compression. Thin Wall Struct 2010; 48(9): 709–17.

[35] Cardoso DCT, Harries KA, Batista E de M. Closed-form equations for compressive local buckling of pultruded thin-walled sections. Thin Wall Struct 2014; 79: 16–22.

[36] Bazant ZP, Cedolin L. Stability of structures: elastic, inelastic, fracture and damage theories. New York: Oxford University Press; 1991.

[37] Cardoso DCT, Harries KA, Batista E de M. Compressive local buckling of pultruded GFRP I-sections: Development and numerical/experimental evaluation of an explicit equation. J Compos Constr 2015; 19(2), DOI: 10.1061/(ASCE)CC.1943-5614.0000501.

[38] Bank LC, Gentry TR, Nadipelli M. Local buckling of pultruded FRP beams—Analysis and design. J Reinf Plast Compos 1996; 15(3): 283–94.

[39] Creative Pultrusions. The new and improved Pultex® pultrusion design manual of standard and custom fiber reinforced polymer structural profiles. Vol. 5, Alum Bank: Creative Pultrusions; 2015.

[40] Vinson JR, Chou TW. Composite materials and their use in structures. New York: John Wiley & Sons; 1975.

[41] ABAQUS 6.13-4. Abaqus Analysis User's Manual, Dassault Systemes Simulia Corp. Rising Sun Mills, 166 Valley Street, Providence, RI 02909-2499, USA.

A closed-form equation for the local buckling moment of pultruded FRP I-beams in major-axis bending

Francesco ASCIONE,[*a] Luciano FEO,[*b] Marco LAMBERTI,[*c]

Fabio MINGHINI,[**d] Nerio TULLINI[**e]

[*] *Department of Civil Engineering, University of Salerno,*

Via Giovanni Paolo II 132, Fisciano (SA), Italy

[**] *Department of Engineering, University of Ferrara,*

Via Giuseppe Saragat 1, Ferrara, Italy

[a] Corresponding author. E-mail: fascione@unisa.it

[b] E-mail: l.feo@unisa.it

[c] E-mail: malamberti@unisa.it

[d] E-mail: fabio.minghini@unife.it

[e] E-mail: nerio.tullini@unife.it

LIST OF FIGURES

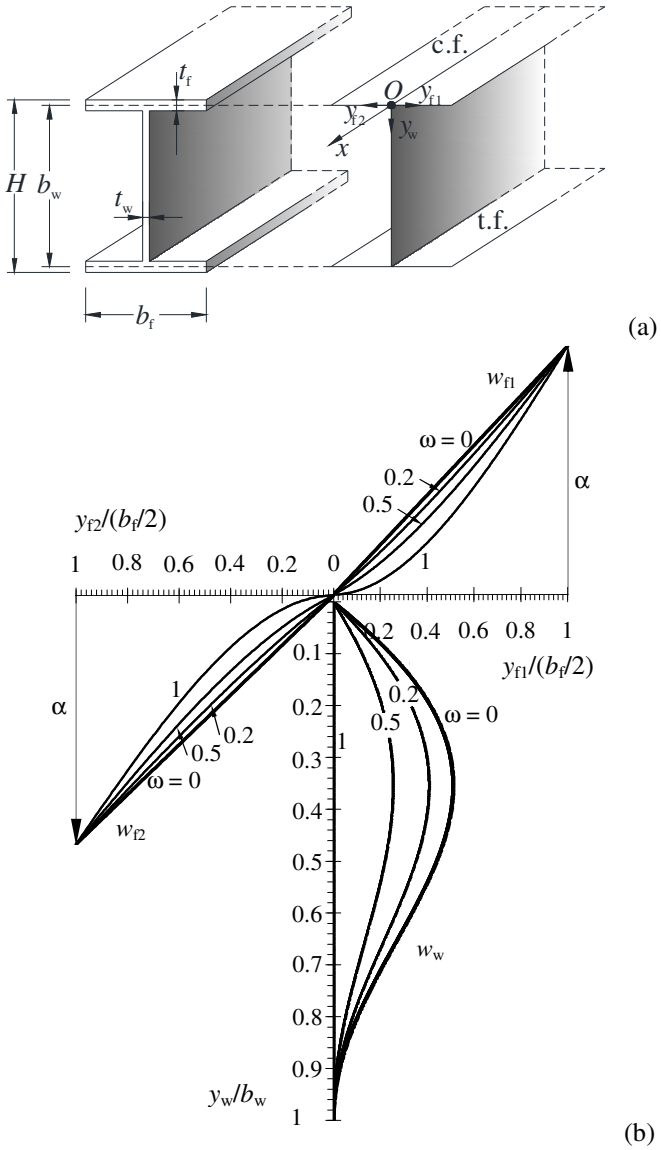

Fig. 1. PFRP I-shaped profile: (a) cross-section dimensions and definition of the local coordinate systems for the web and compression flange (c.f.); and (b) cross-sectional view of the assumed buckled shapes for ω = 0, 0.2, 0.5, and 1.

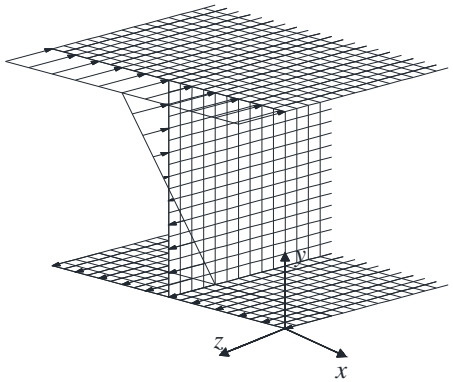

Fig. 2. Normal stress distribution applied at one end section to reproduce major-axis bending.

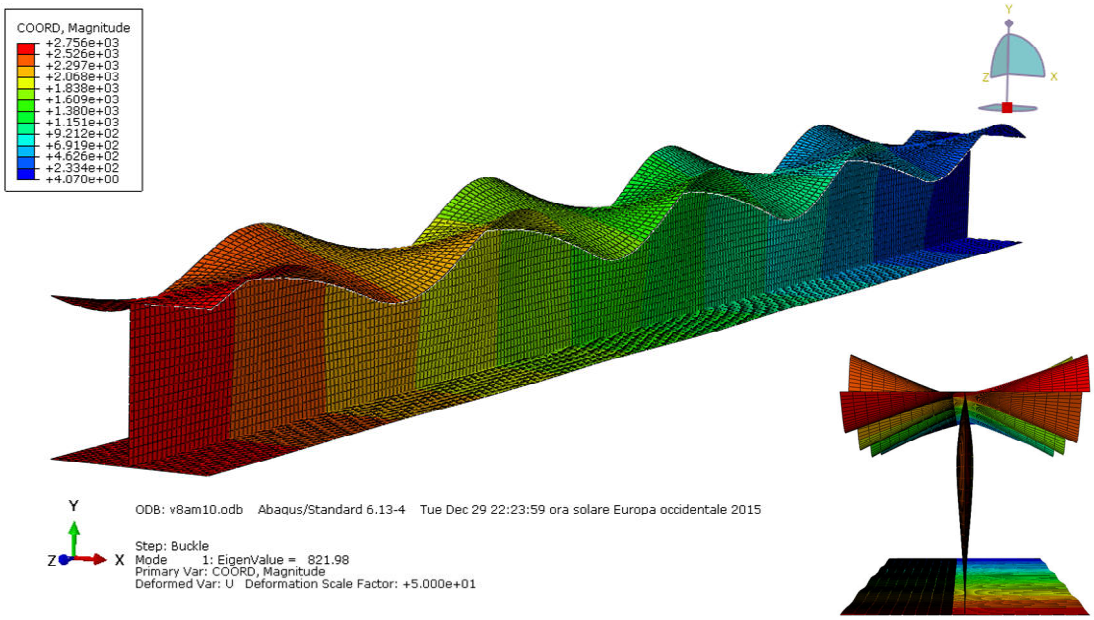

Fig. 3. Typical local buckling shape obtained from the FE analysis.

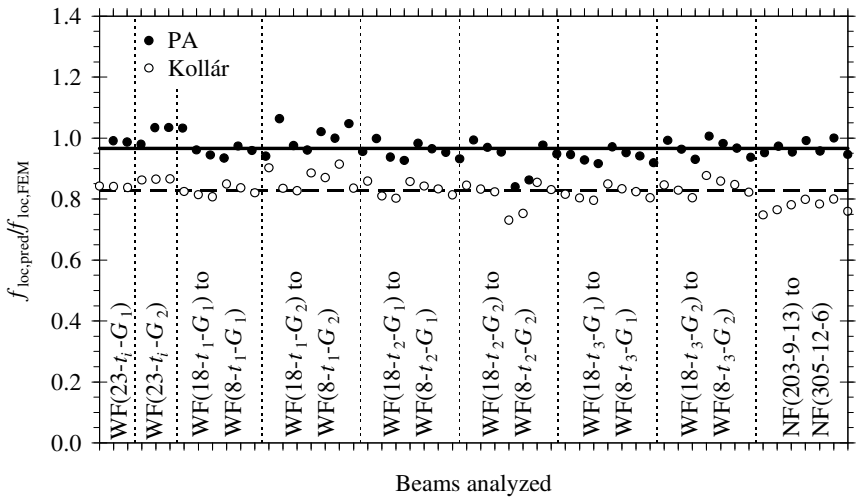

Fig. 4. Ratio of the predicted ($f_{loc,pred}$) to the FE-computed local buckling stress ($f_{loc,FEM}$) for the beams analyzed. Comparison between present analysis (PA) and Kollár's equation.

A closed-form equation for the local buckling moment of pultruded FRP I-beams in major-axis bending

Francesco ASCIONE,[*a] Luciano FEO,[*b] Marco LAMBERTI,[*c]

Fabio MINGHINI,[**d] Nerio TULLINI[**e]

[*] *Department of Civil Engineering, University of Salerno,*

Via Giovanni Paolo II 132, Fisciano (SA), Italy

[**] *Department of Engineering, University of Ferrara,*

Via Giuseppe Saragat 1, Ferrara, Italy

[a] Corresponding author. E-mail: fascione@unisa.it

[b] E-mail: l.feo@unisa.it

[c] E-mail: malamberti@unisa.it

[d] E-mail: fabio.minghini@unife.it

[e] E-mail: nerio.tullini@unife.it

LIST OF TABLES

Table 1. Ratios $r_{Ko} = M_{loc,Ko}/M_{loc,exp}$ (reciprocals of the values reported in [28]) and $r_{PA} = M_{loc,PA}/M_{loc,exp}$ of predicted to experimental buckling moments ($M_{loc,exp}$), with $M_{loc,Ko}$ and $M_{loc,PA}$ indicating buckling moments provided by Kollár's equation and the present analysis, respectively.

Beam ID[(a)]	$H=b_f$ [mm]	$t_f=t_w$ [mm]	E_L[(b)] [GPa]	E_T[(b)] [GPa]	G_{LT}[(b)] [GPa]	υ_{LT}[(b)] [–]	L [m]	W_{max} [$10^5\times mm^3$]	$M_{loc,exp}$[(b)] [kNm]	r_{Ko}[(b)] [–]	r_{PA} [–]
V8A	203.2	9.53	24.6	10.3	3.7	0.33	2.74	4.07	30.62	0.927	1.075
V8B	203.2	9.53	24.6	10.3	3.7	0.33	2.74	4.07	33.89	0.837	0.971
V81	203.2	9.53	24.6	10.3	3.7	0.33	2.74	4.07	33.10	0.857	0.994
V82	203.2	9.53	24.6	10.3	3.7	0.33	2.74	4.07	33.22	0.854	0.991
V83	203.2	9.53	24.6	10.3	3.7	0.33	2.74	4.07	33.56	0.846	0.981
V84	203.2	9.53	24.6	10.3	3.7	0.33	2.74	4.07	30.73	0.923	1.071
V87	203.2	12.7	24.6	10.3	3.7	0.33	2.74	5.20	67.00	0.967	1.119
V88	203.2	12.7	24.6	10.3	3.7	0.33	2.74	5.20	68.69	0.943	1.091
P81	203.2	9.53	24.0	7.5	2.6	0.31	2.74	4.07	33.56	0.659	0.761
P82	203.2	9.53	24.0	7.5	2.6	0.31	2.74	4.07	34.01	0.650	0.751
									Mean	**0.846**	**0.981**
									COV	**0.131**	**0.131**

[(a)] Capital letters V and P in the beam ID refer to vinylester and polyester resins, respectively.
[(b)] For details on material properties and experimental results, see [28, 38].

Table 2. Expressions for the elastic constants and parameters used in Eqs. (11)–(14).

Elastic constants (i = f, w)	
$D_{11,i}$	$E_{L,i}t_i^3/12(1-\upsilon_{LT,i}\upsilon_{TL,i})$
$D_{22,i}$	$E_{T,i}t_i^3/12(1-\upsilon_{LT,i}\upsilon_{TL,i})$
$D_{12,i}$	$\upsilon_{LT,i}D_{22,i}$
$D_{66,i}$	$G_{LT,i}t_i^3/12$
$D_{33,i}$	$D_{12,i} + 2D_{66,i}$
Inhomogeneity and anisotropy ratios	
c_{11}	$D_{11,f}/D_{11,w}$
c_{22}	$D_{22,f}/D_{22,w}$
c_{12}	$D_{11,f}/D_{22,w}$
c_{122}	$D_{12,f}/D_{22,w}$
c_{62}	$2D_{66,f}/D_{22,w}$
c_{32}	$D_{33,f}/D_{22,w}$
$c_{12,w}$	$D_{11,w}/D_{22,w}$
$c_{32,w}$	$D_{33,w}/D_{22,w}$
ω–functions	
$F_{\omega1}$	$(2\pi^2-3)(\omega-1)^2$
$F_{\omega2}$	$F_{\omega1} + 36(\omega-1)^2$
$F_{\omega3}$	$140 - 49\omega+8\omega^2$
$F_{\omega4}$	$F_{\omega1} - (\pi^2+3)(\omega-1)^2$
$F_{\omega5}$	$F_{\omega1} + 6(\omega-1)^2$

Table 3. Convergence test for beam V8A of Table 1: number of subdivisions along each of the flanges (n_f), web (n_w), and span length (n_L); total number of FEs [$n_{el} = (2n_f + n_w)n_L$]; and corresponding critical stress for six FE models with increasing mesh refinement.

Mesh #	n_f	n_w	n_L	n_{el}	$f_{loc,FEM}$ [MPa]
1	8	8	110	2640	87.33
2	10	10	137	4110	86.82
3	14	12	183	7320	86.50
4	16	16	228	10944	86.34
5	18	16	249	12948	86.29
6	20	18	274	15892	86.25

Table 4. Ratios $r_{f,exp} = f_{loc,exp}/f_{loc,FEM}$ and $r_{f,PA} = f_{loc,PA}/f_{loc,FEM}$, with $f_{loc,exp}$, $f_{loc,PA}$, and $f_{loc,FEM}$ indicating local buckling stresses provided by experiments [28], the present analysis, and FE models, respectively.

Beam ID	$f_{loc,FEM}$ [MPa]	$f_{loc,exp}$ [MPa] [(a)]	$f_{loc,PA}$ [MPa] [(b)]	$r_{f,exp}$	$r_{f,PA}$
V8A	86.25	75.32	80.97	0.946	1.017
V8B	86.25	83.36	80.97	1.047	1.017
V81	86.25	81.42	80.97	1.023	1.017
V82	86.25	81.71	80.97	1.026	1.017
V83	86.25	82.55	80.97	1.037	1.017
V84	86.25	75.59	80.97	0.949	1.017
V87	154.80	128.82	144.08	1.067	1.193
V88	154.80	132.07	144.08	1.094	1.193
P81	66.69	82.55	62.86	1.337	1.018
P82	66.69	83.66	62.86	1.355	1.018
			Mean	**1.088**	**1.053**
			COV	**0.132**	**0.070**

[(a)] Obtained from $f_{loc,exp} = M_{loc,exp}/W_{max}$ with $M_{loc,exp}$ and W_{max} reported in Table 1.
[(b)] $f_{loc,PA} = r_{PA}M_{loc,exp}/W_{max}$ with r_{PA} also reported in Table 1.

Table 5. Mechanical properties of the 48 WF-section beams investigated. For all beams $H = b_f = 203.2$ mm, $E_{L,f} = 23$ GPa, and $\upsilon_{LT,f} = \upsilon_{LT,w} = 0.33$.

Beam ID	$E_{T,f}$ [GPa]	$E_{L,w}$ [GPa]	$E_{T,w}$ [GPa]	$t_f = t_w = t_i$ (i = 1, 2, 3) t_1 [mm]	t_2 [mm]	t_3 [mm]	$G_{LT,f} = G_{LT,w} = G_j$ (j=1, 2) G_1 [GPa]	G_2 [GPa]
WF(23-t_i-G_j)	23.0	23.0	23.0	6.53	9.53	12.7	4.0	2.3
WF(18-t_i-G_j)	18.4	23.0	15.3	6.53	9.53	12.7	4.0	2.3
WF(15-t_i-G_j)	15.3	23.0	11.5	6.53	9.53	12.7	4.0	2.3
WF(13-t_i-G_j)	13.1	23.0	9.2	6.53	9.53	12.7	4.0	2.3
WF(11-t_i-G_j)	11.5	19.0	15.3	6.53	9.53	12.7	4.0	2.3
WF(10-t_i-G_j)	10.2	19.0	11.5	6.53	9.53	12.7	4.0	2.3
WF(9-t_i-G_j)	9.2	19.0	9.2	6.53	9.53	12.7	4.0	2.3
WF(8-t_i-G_j)	8.4	19.0	6.0	6.53	9.53	12.7	4.0	2.3

Table 6. Mechanical properties of the seven NF-section beams investigated. For all beams $\upsilon_{LT,f} = \upsilon_{LT,w} = 0.33$.

Beam ID	H [mm]	b_f [mm]	t_f=t_w [mm]	$E_{L,f}$ [GPa]	$E_{T,f}$ [GPa]	$E_{L,w}$ [GPa]	$E_{T,w}$ [GPa]	$G_{LT,f}$ = $G_{LT,w}$ [GPa]
NF(203-9-13)	203.2	101.6	9.53	23.0	13.1	23.0	13.1	4.0
NF(203-9-9)	203.2	101.6	9.53	23.0	13.1	19.0	9.2	4.0
NF(203-12-13)	203.2	101.6	12.7	23.0	13.1	23.0	13.1	4.0
NF(254-9-13)	254	127	9.53	23.0	13.1	19.0	13.1	4.0
NF(254-12-9)	254	127	12.7	23.0	13.1	19.0	9.2	4.0
NF(305-12-13)	305	152	12.7	23.0	13.1	19.0	13.1	3.5
NF(305-12-6)	305	152	12.7	17.2	6.2	17.2	6.2	2.9